J Fluoresc (2015) 25:1757–1762
DOI 10.1007/s10895-015-1663-5

ORIGINAL ARTICLE

Structural and Luminescence Properties of Sm^{3+} Doped TTB -Type $BaTa_2O_6$ Ceramic Phosphors

Mete Kaan Ekmekçi[1] · Mustafa İlhan[2] · Ali Sadi Başak[1] · Sabahattin Deniz[3]

Received: 4 June 2015 / Accepted: 14 September 2015 / Published online: 26 September 2015

Abstract Pure and 0.5 to 10 mole% Sm^{3+} doped TTB (tetragonal tungsten bronze)-type $BaTa_2O_6$ ceramic phosphor was produced by the solid state reaction method which performed at 1425 °C for 20 h. XRD and SEM analysis indicated single TTB phase for undoped and 0.5 to 10 mole% Sm^{3+} doped $BaTa_2O_6$ structures. SEM also showed that the $BaTa_2O_6$ grain size decreased with the increasing content of Sm^{3+}. Optical analysis indicated significant emissions in the visible spectral region as green (λ=562.7 nm) and orange-reddish (λ=597.1 nm). The emission intensity increased with the increasing doping concentration up to 2.5 mole%, and then decreased due to the concentration quenching effect.

Keywords TTB-type $BaTa_2O_6$ · Photoluminescence · Solid state reaction

Introduction

The technology of optical materials has rapidly developed over the last two decades. Materials doped with trivalent rare earth ions (RE: Eu^{3+}, Sm^{3+}, Y^{3+}, Dy^{3+} etc.) attracted considerable interest due to their photoemission throughout the visible spectral range [1]. The bright luminescence of these phosphors made possible a new generation of lighting and display devices with good thermal and chemical stability, and safety of use [2, 3].

Ceramic oxides are known to exhibit excellent mechanical, thermal, electrical and optical properties which makes them good host materials for various rare earth dopants [4, 5]. The resulting ceramic phosphors generally exhibit bright emission, high homogeneity and low thermal conductivity leading to low power consumption and long service life. Ceramic phosphors are used in many areas such as fluorescent lighting devices, electroluminescent devices, plasma displays; color TVs, LEDs, lasers, and optical storage systems [6–11]. $BaTa_2O_6$ is one of the well-known compounds in BaO-Ta_2O_5 system which has been studied recently because of its dielectric and photocatalytic properties [12–17]. $BaTa_2O_6$ has three crystal structures as orthorhombic, tetragonal and hexagonal [18].

TTB crystal structure is related to that of potassium tungstate ($K_{0.475}WO_3$) [19]. Ceramic oxides with such structure exhibit non-linear behavior under the influence of mechanical stress and when external electric and magnetic fields are applied [20]. The crystal structure of TTB contains open channels along the c-direction and has more cationic sites compared to that of the perovskite structure, five compared to two, allowing the incorporation of atomic additives along the channels and/or in vacant cationic sites that may be occupied with dopants based on their legacy and ionic radii [21].

The synthesis of $BaTa_2O_6$ ceramic material has been carried out by a number of methods: ceramic flux [22–24], conventional solid state method [25, 26], precipitation and mechanochemical synthesis [27, 28].

4f valance electrons of rare earth ions are shielded by $5s^2$ and $5p^6$ outer electrons and thus are weakly affected by the crystal field [29]. Therefore, electronic transitions involved in the luminescence are largely host independent, and typically

✉ Mete Kaan Ekmekçi
mekmekci@marmara.edu.tr

[1] Art and Science Faculty, Marmara University, Kadıköy 34722, Istanbul, Turkey

[2] Faculty of Engineering, Marmara University, Kadıköy 34722, Istanbul, Turkey

[3] Faculty of Technology, Marmara University, Kadıköy 34722, Istanbul, Turkey

exhibit sharp peaks in emission spectra. Incorporation of Sm^{3+} ions into the crystal lattice, and electronic transitions resulting from photo excitation, yield two main emission bands at 563 nm (magnetic dipole transition of ion $^4G_{5/2} \rightarrow {}^6H_{5/2}$), and 597 nm (partly magnetic and partly a forced electric-dipole transition $^4G_{5/2} \rightarrow {}^6H_{7/2}$) [30–32].

In this study, detailed microstructural characterization of the sintered samples was performed using the XRD and SEM techniques. Moreover, microstructural characterization, the luminescence properties and the optical properties of Sm^{3+} doped $BaTa_2O_6$ ceramic were investigated and discussed in detail.

Materials and Methods

Materials

$BaCO_3$ (Sigma-Aldrich, with purity of 99 %) and Ta_2O_5 (Alfa Aesar, with purity of 99.9 %) Sm_2O_3 (Alfa Aesar, with of purity 99.9 %) powders were used as starting materials.

Methods

Synthesis

Undoped and Sm^{3+} doped $BaTa_2O_6$ ceramics were synthesized by the conventional solid state reaction method. Initially, Sm_2O_3, $BaCO_3$ and Ta_2O_5 powder mixtures with stoichiometric ratio ranging between 0.5 and 10 mole% Sm_2O_3 content were prepared. The powder mixtures were homogenized in agate mortar with the addition of acetone for 10 min. Then they placed in a high temperature furnace for heat treatment at 1425 °C for 20 h in the air atmosphere.

XRD and SEM Analysis

Phases composition of oxides were determined by X-ray diffractometer (XRD, Rigaku Corp., D-MAX 2200) using Cu Kα radiation between 2θ=15–60° at 2°/min and Ni filter. The morphology of the heat treated ceramic powders was investigated by Scanning Electron Microscopy (SEM, JEOL Ltd., JSM-5910LV) equipped with EDS (OXFORD Industries INCA x-Sight 7274; 133-eV resolution 5.9 keV) after gold coating.

Fluorescence Measurements

Photoluminescence measurements were performed by Scinco, floromaster-FS/2 model fluorescence spectrofluorometer. All emission and excitation spectra were acquired at photon multiplier tube (PMT) voltage of 600 V. All measurements were taken at room temperature.

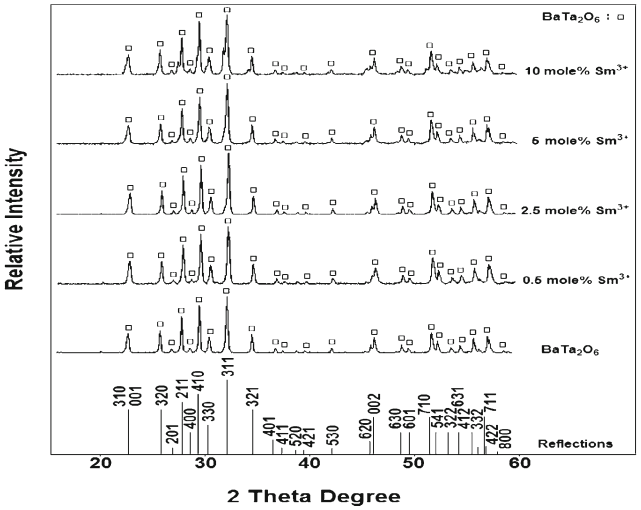

Fig. 1 X-ray diffraction patterns of $BaTa_2O_6$ and Sm^{3+} doped $BaTa_2O_6$ structures

Results and Discussion

XRD and SEM-EDS Analysis Sm^{3+} Doped $BaTa_2O_6$ Powders

Figure 1 shows XRD patterns of pure $BaTa_2O_6$ and Sm^{3+} doped samples. According to XRD results, single phase $BaTa_2O_6$ (JCPDS card No.17-0793) was maintained up to about 10 mole% Sm_2O_3 [16]. XRD analysis also revealed that powder sample was crystallized in tetragonal symmetry with space group P4/mbm having the tetragonal tungsten bronze (TTB) type structure. It was reported by Layden that, $BaTa_2O_6$

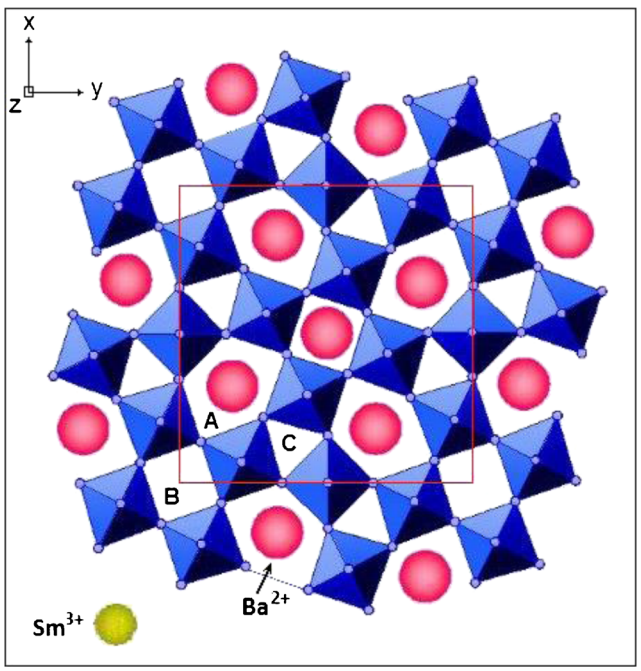

Fig. 2 The illustration of possible Sm^{3+} ions occupancy states within TTB-$BaTa_2O_6$ structure

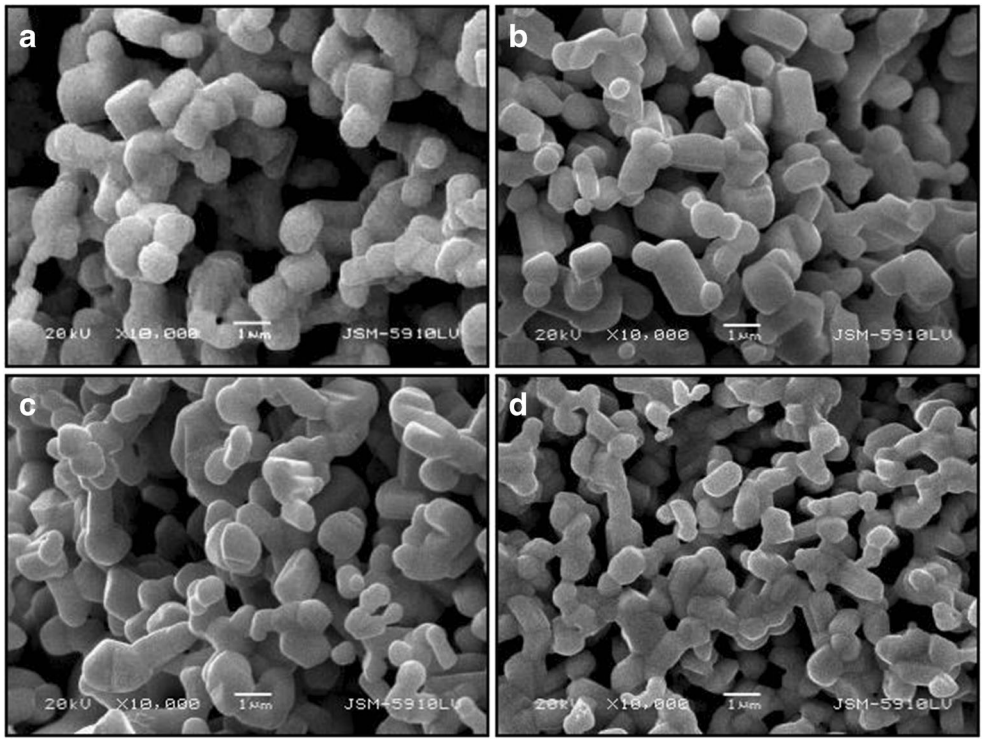

Fig. 3 SEM seconder electron micrographs of (**a**) 0.5, (**b**) 2.5, (**c**) 5 and 10 mole% Sm^{3+} doped TTB-$BaTa_2O_6$ structures

has a tetragonal structure with cell parameters of a=12.52 Å, c=3.956 Å and V=620.10 (Å) [18].

The TTB structure has the general formula of $A_2BC_2M_5X_{15}$, where X=O is anion, M=Ta is octahedral cation, and A, B and C are cations [20]. TTB is composed of a framework of adjacent octahedral sharing corners. In the TTB–$BaTa_2O_6$, the pentagonal A sites are located by Ba^{2+}, the square B sites by Ba^{2+} or empty, whereas the small triangular (C) sites are empty. A, B and C corresponds to the cationic sites having the coordination numbers of 15, 12 and 9 respectively. Based on the ion's radius and valence, the square (B) sites in the framework might be occupied by smaller Sm^{3+} ions which have an ionic radius of 1.24 Å compared to 1.61 Å for Ba^{2+} [30]. Also, Sm^{3+} cations might easily enter into the larger pentagonal (A) sites which were available for Ba^{2+} cations [16]. On the other hand, the vacant triangular (C) sites were too small to accommodate the Sm^{3+} cations. Sm^{3+} doped $BaTa_2O_6$ structure could be illustrated as shown in Fig. 2.

Figure 3 gives the SEM micrographs of doped powders with 0.5, 2.5, 5 and 10 mole% Sm^{3+} content. Grain size decreased with increasing Sm^{3+} concentration and changed between 0.5 and 3.0 μm for the doped powders. Also, grains exhibited nearly round and cornered shapes for powders. SEM-EDS analysis of grains of the 2.5 mole% Sm^{3+} doped

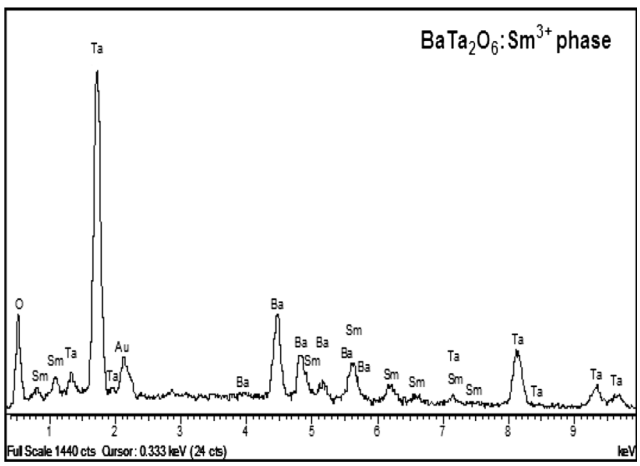

Fig. 4 EDS analysis spectrum of 2.5 mole% Sm^{3+} doped $BaTa_2O_6$ phase

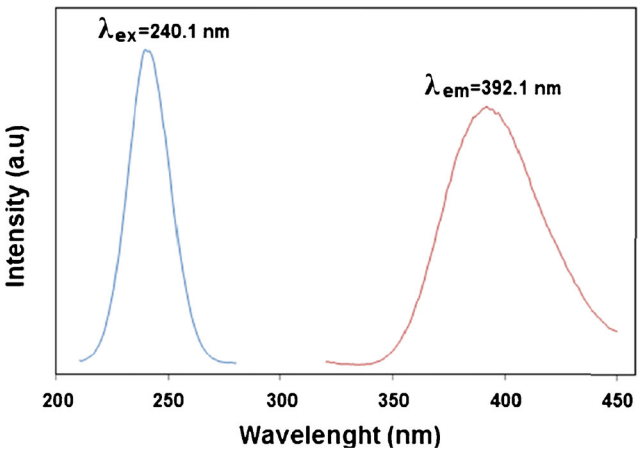

Fig. 5 The excitation and emission peaks of $BaTa_2O_6$ host at λ_{ex}= 240.1 nm and at λ_{em}=392.1 nm, respectively

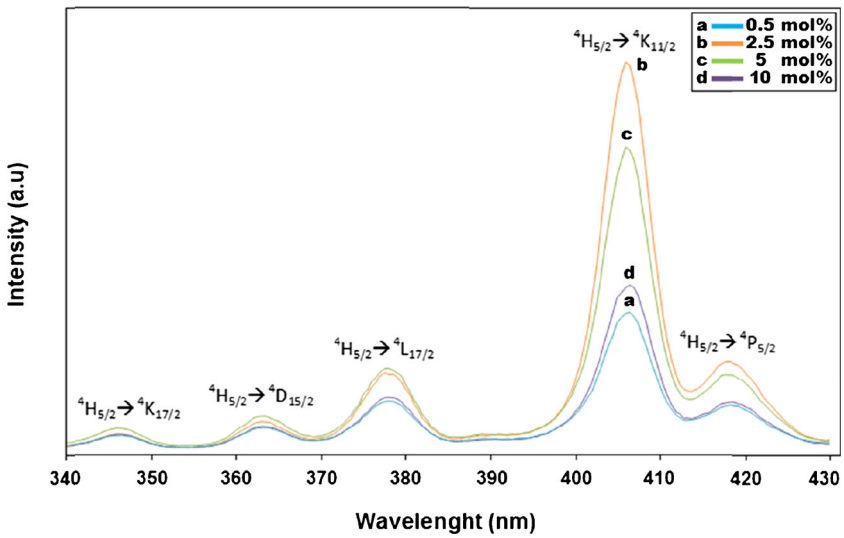

Fig. 6 Excitation spectra of Sm^{3+} doped $BaTa_2O_6$:Sm^{3+} phosphors at λ_{em}=597.1 nm

powder is shown in Fig. 4. EDS analysis revealed the chemical composition of the grains which consistent with the SEM and XRD results. Based on the XRD and SEM analyses results, although the incorporation of Sm^{3+} ions did not cause the change in the single phase structure of $BaTa_2O_6$ up to 10 mole% concentration, the insertion of Sm^{3+} ions will affect the charge compensation in the structure [16]. Therefore, a changing charge balance in the $BaTa_2O_6$ lattice could be based on mostly the loss of Ba^{2+} cations due to evaporation and small amount of Ta^{5+} cations related to the distortion of TaO_6 [16].

Optical Properties of Sm^{3+} Doped $BaTa_2O_6$ Phosphors

Photoluminescent properties of $BaTa_2O_6$ host were reported previously [16]. TTB-$BaTa_2O_6$ showed the broad excitation band at 240.1 nm and emission band at 392.1 nm as presented in Fig. 5. The Ta-O vibrations occur at lower frequencies in $BaTa_2O_6$ structure which is special to the tantalates [19]. Therefore, it is possible to state that a small amount of absorption energy of $BaTa_2O_6$ could not be converted into the non-radioactive energy due to the strong emission of host. $BaTa_2O_6$ could also have low gap energy due to low vibrational phonon energy which is less than that of niobates. Based on the results, strong charge-transfer absorption of tantalates was possibly induced by weak interactions among TaO_6 octahedrals. This promoted the excitation energy to Re^{3+} ion centers that within the $BaTa_2O_6$ host [16].

Figure 6 shows the excitation spectra of $BaTa_2O_6$:xSm^{3+} (x=0.5, 2.5, 5 and 10 mole%) phosphors measured at emission wavelength of 597.1 nm between 340 and 430 nm spectral range. Five excitation bands were identified corresponding to the known transitions: $^4H_{5/2}\rightarrow{}^4K_{17/2}$, $^4L_{17/2}$ (347 nm),

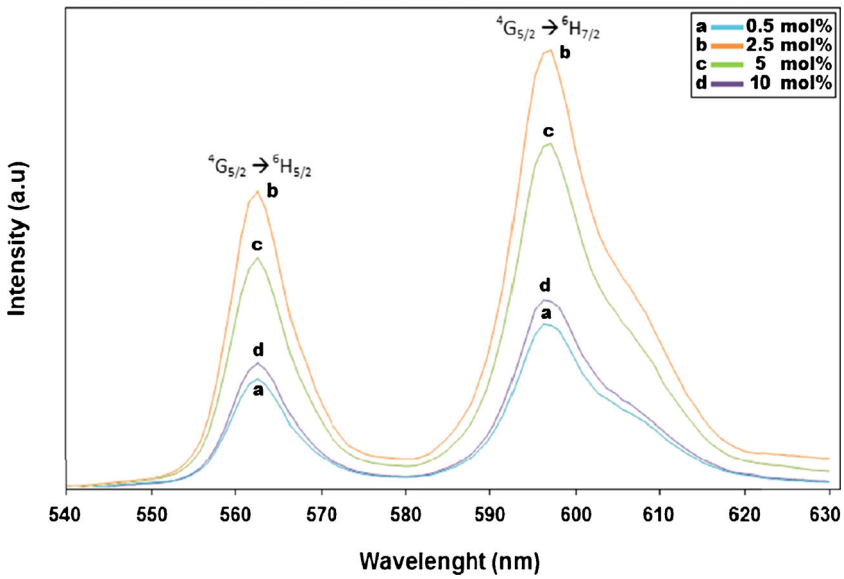

Fig. 7 Emission spectra of Sm^{3+} doped $BaTa_2O_6$:Sm^{3+} phosphors at λ_{em}=406 nm

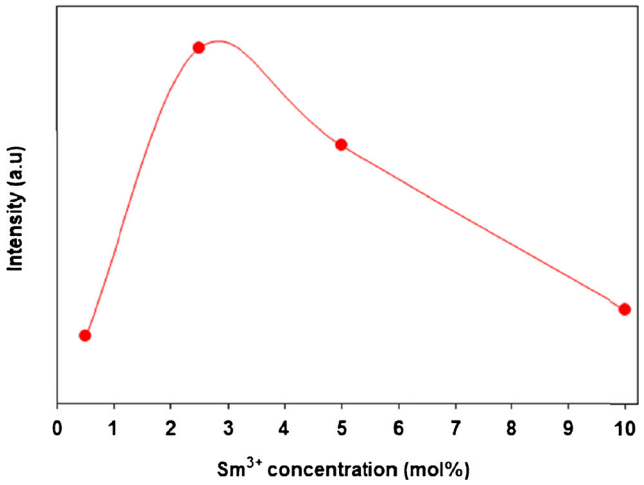

Fig. 8 Emission intensity dependence of Sm^{3+} concentration for $BaTa_2O_6:Sm^{3+}$ phosphors at λ_{em}=597.1 nm

$^4H_{5/2}\rightarrow{}^4D_{15/2}$, $^6P_{15/2}$ (364 nm), (364nm), $^4H_{5/2}\rightarrow{}^4L_{17/2}$ (377 nm), $^4H_{5/2}\rightarrow{}^4K_{11/2}$ (406 nm), $^4H_{5/2}\rightarrow{}^4P_{5/2}$, $^6P_{5/2}$, (420 nm). The assignments of the different excitation bands were identified on the basis of Dieke's energy level diagram [31].

Figure 7 shows emission spectra of $BaTa_2O_6:xSm^{3+}$ (x= 0.5, 2.5, 5 and 10 mole%) phosphors excited at 406 nm which considered due to its sharpness and high intensity. Photoluminescence of $BaTa_2O_6:Sm^{3+}$ phosphors exhibited two typical emission transitions $^4F_{9/2}\rightarrow{}^6H_{15/2}$ and $^4F_{9/2}\rightarrow{}^6H_{13/2}$ as the green emission at 562.7 nm and orange-reddish emission at 597.1 nm, respectively.

Figure 8 shows the dependence of emission spectra of $BaTa_2O_6:Sm^{3+}$ phosphors on doping concentration which excited at 406 nm. The luminescence intensity increased with increasing Sm^{3+} concentration of up to 2.5 mole%, and then decreased because of concentration quenching effect. This phenomenon can be explained by host properties and RE^{3+} concentration. Firstly, excitation energy can be transferred to the lattice

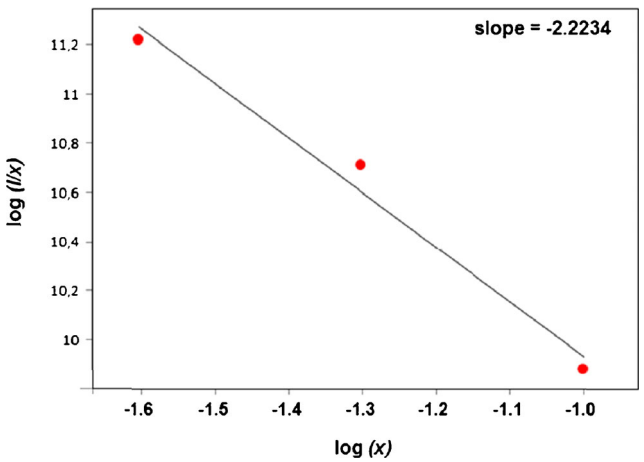

Fig. 9 Relation between the $\log_{10}(I/x)$ and $\log_{10}(x)$ of Sm^{3+} for $BaTa_2O_6:Sm^{3+}$ phosphors

vibrations because of defects or impurity ions which depend on the phonon spectrum of the host lattice. Secondly, excitation energy depends on RE^{3+} concentration which is transferred between RE^{3+} ions where emission state is lost by cross relaxation mechanism [27]. The increasing of Sm^{3+} concentration promotes nonradiative energy transfer between Sm^{3+} ions. On the other hand, the multiphonon relaxation of tantalates is very low due to low vibration energy which decreases the non-radiative energy [16, 19]. Therefore, excitation energy transfer strongly depends on the critical concentration of Sm^{3+} ions. The critical distance for energy transfer (R_c) in $BaTa_2O_6:Sm^{3+}$ can be estimated from Blasse's equation [32] (1):

$$R_c \approx 2\left(\frac{3V}{4\pi x_c N}\right)^{1/3} \quad (1)$$

where the structural parameters namely unit cell volume (V), the number of available sites for the dopant in the unit cell (N) and critical concentration of dopant (X_c). For the $BaTa_2O_6:Sm^{3+}$ phosphor, X_c=0.025, V=620.10 (Å)^3 and N=10 [32]. The R_c of Sm^{3+} in $BaTa_2O_6:Sm^{3+}$ was calculated as 16.80 Å. The nonradiative energy transfer of the luminescence of phosphors is based on resonance transfer by electric multipole–multipole interaction or exchange interaction. According to Blasse's theory when the critical distance is larger than 5 Å, only a multipole–multipole interaction is important where the exchange interaction becomes ineffective. When the distance is shorter than 5 Å, the exchange interaction becomes effective. Therefore, effective quenching mechanism of $BaTa_2O_6:Sm^{3+}$ phosphor was the multipolar interaction since R_c value is 16.80 Å.

Type of the nonradioactive energy transfer can be determined according to Van Uitert that if the energy transfer occurs among the same sorts of activators, the strength or type of the multipolar interaction can be determined from the change of the emission intensity and per concentration ion level that follows the Eq. (2): [32]

$$I/x = K\left[1+\beta(x)^{\theta/3}\right]^{-1} \quad (2)$$

In this equation (x) is the phosphor concentration that is not less than the critical concentration. The (I/x) is the emission intensity (I) per phosphor (x). The (K) and (β) are the constants for the same excitation condition for a phosphor crystal. The (θ) value indicates the electric multipolar character where $\theta=3$ for the energy transfer among the nearest-neighbor ions (exchange interaction), while $\theta=6$ for dipole–dipole (d–d), $\theta=8$ for dipole–quadrupole (d–p) and $\theta=10$ for quadrupole–quadrupole (q–q) interactions. Assuming that $\beta(x)^{\theta/3} \gg 1$, Eq. (2) can be simplified as follows (Fig. 9):

$$\log(I/x) = K' - \theta/3 \log x \left(K' = \log K - \log\beta\right) \quad (3)$$

Conclusions

Pure and Sm^{3+} doped single phase TTB-$BaTa_2O_6$ ceramics were synthesized by the conventional solid state reaction method at 1425 °C for 20 h. Incorporation of samarium ions into the vacant sites of TTB network significantly increased emission intensity in the visible spectral range. Both XRD and SEM results indicated single phase for the 0.5 to 10 mole% Sm_2O_3 doped powders. Increasing the doping level up to 2.5 mole% resulted in a slight distortion leading to lattice constant expansion while maintaining the TTB network symmetry. Moreover, powder grain size decreased with the increase in the Sm_2O_3 doping content. The emission intensity increased with increasing doping concentration up to 2.5 mole%. Beyond this, concentration quenching phenomenon was observed.

Acknowledgments The authors would like to thanks to Marmara University Research Fund (BAPKO) for supporting this research. Project No. FEN-A-150513-0167

References

1. Castro Y, Julian B, Boissiére C, Viana B, Amenitsch H, Grosso D, Sanchez C (2007) Synthesis, characterization and optical properties of Eu_2O_3 mesoporous thin films. Nanotechnology 18:55705
2. Wang D, Yin QR, Li YX, Wang MQ (2002) Concentration quenching of Eu^{2+} in $SrO{\cdot}Al_2O_3{:}Eu^{2+}$ phosphor. J Lumin 97:1–6
3. Chang H, Lenggoro IW, Ogi T, Okuyama K (2005) Direct synthesis of barium magnesium aluminate blue phosphor particles via a flame route. Mater Lett 59:1183
4. Yang HM, Shi JX, Gong ML (2005) A novel red emitting phosphor Ca_2SnO_4: Eu^{3+}". J Solid State Chem 178:917–920
5. Fang TH, Hsiao YJ, Chang YS, Chang YH (2006) Photoluminescent characterization of $KNbO_3$: Eu^{3+}. Mater Chem Phys 100:418–422
6. Welker T (1991) Recent developments on phosphors for fluorescent lamps and cathode-ray tubes. J Lumin 48–49:49–56
7. Vedda A, Martini M, Nikl M, Mihokova E, Nitsch K, Solovieva N, Karagulian F (2002) Optical absorption and thermoluminescence of Tb^{3+}-doped phosphate scintillating glasses. J Phys Condens Matter 14:7417
8. Nakamura S, Fasol G (1997) The blue laser diode: GaN based light emitters and laser. Springer, Berlin
9. Levine AK, Palilla FC (1994) A new, highly efficient red-emitting cathodoluminescent phosphor (YVO_4:Eu) for color television. Appl Phys Lett 5:5118–5120
10. Rao RP (2005) Tm^{3+} activated lanthanum phosphate: a blue PDP phosphor. J Lumin 113:271–278
11. Yan ZG, Yan CH (2008) Controlled synthesis of rare earth nanostructures. J Mater Chem 18:5046–5059
12. Magneli A (1949) Ark Kemi 1:213–221
13. Simon A, Ravez J (2006) Solid-state chemistry and non-linear tungsten bronzes materials. C R Chim 9:1268–1276
14. Roulland F, Josse M, Castel E, Maglione M (2009) Influence of ceramic process and Eu content on the composite multiferroic properties of the $Ba_{6-2x}\ Ln_{2x}Fe_{1+x}Nb_{9-x}O_{30}$ TTB system. Solid State Sci 1:1709–1716
15. Kovba LM, Lykova LN, Paromova MV, Lopato LM, Shevchenko AV (1977) Barium oxide-tantalum oxide system. Russ J Inorg Chem 22:1544
16. Layden GK (1968) Dielectric and structure studies of hexagonal BaTa2O6. Mater Res Bull 3:349
17. Smolenskii GA, Isupov VA, Agranovskaia AI (1956) Sov Phys 300:1
18. Ichinose N, Shimada T (2006) Effect of grain size and secondary phase on microwave dielectric properties of Ba(Mg1/3Ta2/3)O3 and Ba([Mg, Zn]1/3Ta2/3)O3 systems. J Eur Ceram Soc 26: 1755–1759
19. Lee YH, Kim YS, Kim DH, Oh MH (2007) Conduction mechanisms in barium tantalates films and modification of interfacial barrier height. IEEE Trans Electron Devices 47:71–76
20. Kato H, Kudo A (1998) New tantalate photocatalysts for water decomposition into H_2 and O_2. Chem Phys Lett 295:487–492
21. Layden GK (1967) Polymorphism of $BaTa_2O_6$. Mater Res Bull 2: 533
22. Vanderah TA, Roth RS, Siegrist T, Febo W, Loezos JM, Wong-Ng W (2003) Subsolidus phase equilibria and crystal chemistry in the system BaO–TiO_2–Ta_2O_5. Solid State Sci 5:149–164
23. Mumme WG, Grey IE, Roth RS, Vanderah TA (2007) Contrasting oxide crystal chemistry of Nb and Ta: the structures of the hexagonal bronzes $BaTa_2O_6$ and $Ba_{0.93}Nb_{2.03}O_6$. J Solid State Chem 180: 2429–2436
24. Navale SC, Samuel V, Gaikwad AB, Ravi V (2007) A co-precipitation technique to prepare $BaTa_2O_6$. Ceram Int 33:297–299
25. İlhan M, Mergen A, Yaman C (2011) Mechanochemical synthesis and characterisation of $BaTa_2O_6$ ceramic powders. Ceram Int 37: 1507–1514
26. İlhan M, Mergen A, Yaman C (2013) Removal of iron from $BaTa_2O_6$ ceramic powder produced by high energy milling. Ceram Int 39:5741–5750
27. Speight JG (1999) Lange's handbook of chemistry, 16th edn. The McGraw-Hill Companies, New York
28. Erkmen EZ (2012) Malzeme Karakterizasyonu ve Temel İlkeleri. Yalın Yayıncılık, İstanbul
29. Garciá JS, Bausá LE, Jaque D (2005) An introduction to the optical spectroscopy of inorganic solids. Wiley, England
30. Pang TP, Yang MR, Chen KS (2000) Photoluminescence of ZnS: Sm phosphor prepared in a reductive atmosphere. Ceram Int 26: 153–158
31. Kaur G, Dwivedi Y, Rai SB (2010) Study of enhanced red emission from $Sm(Sal)_3$ Phen ternary complexes in Poly Vinly alcohol film. Opt Commun 283:3441–3447
32. Yerpude AN, Dhoble SJ (2012) Synthesis and photoluminescence properties of Dy^{3+}, Sm^{3+} activated $Sr_5SiO_4Cl_6$ phosphor. J Lumin 132:2975–2978